ELSEVIER

Effect of wall inclination on the mean flow and turbulence characteristics in a two-dimensional wall jet

J. C. S. Lai and D. Lu
Department of Aerospace & Mechanical Engineering, University College,
The University of New South Wales, Australian Defence Force Academy, Canberra, Australia

Mean velocity and turbulence measurements, using hot-wire anemometry, were made up to 20 nozzle widths downstream of a nozzle in a two-dimensional (2-D) wall jet facility in which the angle of inclination of the wall to the nozzle was varied from 0 to 90° for a nozzle exit Reynolds number of 10,000. The effect of the wall angle (β) on the spatial development of the velocity field of the jet has been documented for $\beta = 0°$, 15°, 30°, 45°, and 90°. Results indicate that in the range $0° \leq \beta \leq 45°$, as the wall angle β increases, the centreline velocity decays faster, and the jet spreads faster, resulting in a shorter potential core and increase in jet volume entrainment. The positions of reattachment of the jet to the wall for various β have been deduced from surface pressure measurements and flow visualisation techniques.

Keywords: wall jet; turbulent shear flow; boundary layer; wall angle

Introduction

Wall jets have numerous important engineering applications; one of these is film-cooling in heat transfer. Consequently, substantial efforts have been devoted to studies of wall jets. However, reviews by Launder and Rodi (1981) and Launder (1983) on turbulent wall jets have revealed that despite over 200 publications on the topic, accurate data, particularly on the distribution of turbulence stresses, are lacking, and the physics of the flow is still not well understood. Some of the more recent studies, such as Matsuda et al. (1990), Katz et al. (1992), Zhou and Wygnanski (1993), Hsiao and Sheu (1994), and Schneider and Goldstein (1994), have focused on the flow structures in wall jets. With a very few exceptions, all the measurements thus far were conducted in the fully developed region of the jet where self-preservation is being approached or has already been attained. Because most practical applications involve the near field of wall jets, it is important to study the distribution of velocities and turbulent stresses in these regions. In most practical applications of wall jets, the jet is injected at an angle to a solid boundary; this configuration is referred to as the inclined wall jet.

The first experimental study of an inclined wall jet was reported by Forthman (1934). Deflection of plane jets by adjacent boundaries was also studied by Bourque and Newman (1960) and Newman (1961). Based on dimensional analysis and pressure measurements, Newman showed that, provided the exit Reynolds number is greater than 5500, the nondimensional reattachment distance x_R/h is only a function of β, for $x_R/L < 0.75$. Under these conditions, x_R/h is independent of L/h for $L/h > 25$. By making several assumptions, one of which is that the centreline of the jet is a circular arc with radius r, Newman proposed a flow model (Figure 1) for an inclined wall jet, which expressed x_R/h as a function of β and r. His results seem to be supported by pressure measurements for $\beta > 30°$.

The mean flow characteristics in the near field of an inclined wall jet are of great practical significance in such engineering applications as advanced aerofoil designs, film cooling of turbine blades, gas turbine combustion chamber walls, and deflectors used in air conditioning ducts. While pressure measurements in an inclined wall jet were reported by Newman (1961), and several attempts in modelling the flow to predict the jet reattachment distance were made by such researchers as Bourque (1967) and Perry (1967), the velocity field of an inclined wall jet, particularly, in the near field, has not been fully explored. An inclined wall jet is more complex than a plane wall jet ($\beta = 0°$) due to the influence of the wall angle on the flow as an additional variable. Although the influence of the wall angle on the flow characteristics of an inclined wall jet may appear qualitatively similar to that of diffuser flows, especially in the recirculating flow region, the intrinsic difference between an inclined wall jet flow and diffuser flow is that there is no entrainment in diffuser flows. While very limited hot-wire data were reported by Marsters (1978) for a jet in the neighbourhood of an inclined plane wall, air was allowed to flow through a gap between the jet nozzle and the wall (ventilation) so that there was no recirculation flow region near the wall. Consequently, the flow configuration of Marsters differs significantly from that of Bourque and Newman (1960) and this study, and the results are not directly comparable to this study.

The primary objective of this paper is, therefore, to document the effect of the angle of inclination of the wall to a two-dimen-

Address reprint requests to Dr. J. C. S. Lai, Dept. of Aerospace and Mechanical Engineering, University of New South Wales, Australian, Defence Force Academy, Canberra ACT 2600 Australia.

Received 5 December 1994; accepted 14 February 1996

Int. J. Heat and Fluid Flow 17: 377–385, 1996

655 Avenue of the Americas, New York, NY 10010

0142-727X/96/$15.00
PII S0142-727X(95)00017-1

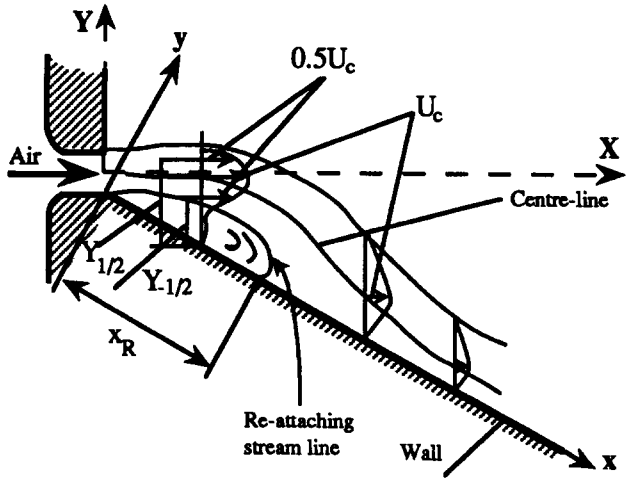

Figure 1 Model for an inclined wall jet (after Newman 1961)

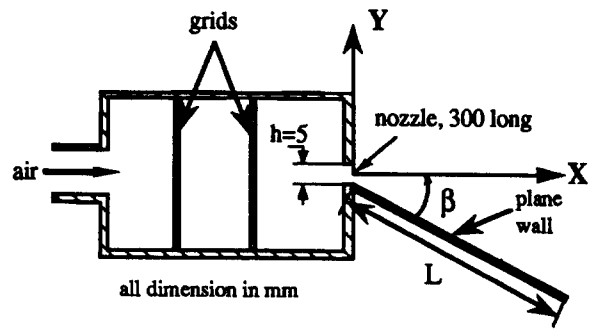

Figure 2 Schematic diagram of setup of inclined wall jet facility

sional (2-D) nozzle on the spatial development of mean velocities and turbulence intensities of the jet for wall angle $\beta = 0°$ (plane wall jet), 15, 30, 45, and 90° (free jet). There is no offset between the wall and the edge of the nozzle.

Apparatus and instrumentation

Measurements were made in a 2-D nozzle facility shown schematically in Figure 2. The jet of air issued into stationary air from a rectangular nozzle with profiles based upon the British Standard BS1042 (1973). The nozzle dimensions were: length $l = 300$ mm, width $h = 5$ mm, giving an aspect ratio of 60. Air from a blower was passed through a series of grids which reduced the turbulence intensity at the nozzle exit for the steady jet to about 0.3% at the centreline, as described by Lai and Simmons (1985). The wall length was $L = 500$ mm, giving $L/h = 100$. Both single and X hot wires, operated at an overheat ratio 1.3 with TSI IFA100 constant temperature anemometer were used to obtain the mean velocities, turbulence intensities, and Reynolds stress in the X and Y directions up to 20 nozzle widths downstream of the nozzle exit, for $\beta = 0°$ (plane wall jet), 15, 30, 45, and 90° (free jet). Hot-wire probes, controlled by an NEC 386/20 computer, were traversed in the X and Y directions by two stepping motors. The exit Reynolds number (based on nozzle width h and exit velocity (U_o) was 10,000. The variation of the ambient temperature was within ± 1°C. The hot wire was calibrated at the nozzle exit of the wall jet facility but with the wall removed. A fourth-order polynomial fit was applied to the relationship between the output voltage of the hot wire and velocity measured with a Pitot tube. The angular sensitivity of the X-wire was calibrated in the same facility, which allowed the X-wire to be rotated through an angular range from -28 to 28° in steps of 2°, where 0° bisects the X-wire. Except at the edge of the jet and near the wall, the uncertainty in the velocity and turbulence intensity measurements is within 2.5 and 5%, respectively. It must be pointed out here that although hot-wire measurements in the recirculating flow region are not valid because of the inability of the hot-wire to discriminate reversed flow, the purpose of this study is to illustrate the general spatial development of an inclined wall jet, excluding the details of the recirculating flow region.

The reattachment of an inclined wall jet to a plane wall was studied by measurement of wall surface pressure distributions using an MKS Baratron 398 HD pressure transducer, a Scanivalve model 48s3, and a MKS Baratron 270B display unit. Flow visualisation techniques using tufts, oil-film, and smoke were also used. The oil was made from a mixture of kerosene, titanium dioxide, and a few drops of oleic acid. The ratio of titanium dioxide to kerosene was approximately 1 : 5 by volume, and the mixture was painted along the wall surface from the wall nozzle to some distance downstream, which covered the reattachment length.

Notation

h	width of two-dimensional nozzle
L	length of wall (Figure 2)
l	length of nozzle
P_0	supply jet pressure
P_∞	static pressure in the surroundings
P_s	wall surface pressure
R_o	nozzle exit Reynolds number based on h and U_o
U	mean X-component velocity
U_c	centreline velocity (maximum X-component velocity at a given X)
U_o	averaged nozzle exit velocity
V	mean Y-component velocity
X	streamwise direction in a rectangular Cartesian coordinate system based at the nozzle exit (Figure 2)
Y	transverse direction in a rectangular Cartesian coordinate system based at the nozzle exit (Figure 2)
$Y_{1/2}$	distance measured in the positive Y direction between the x-axis and the point where the local mean X-component velocity is equal to $U_o/2$ (Figure 1)
$Y_{-1/2}$	distance measured in the negative Y direction between the x-axis and the point where the local mean X-component velocity is equal to $U_o/2$ (Figure 1)
x	streamwise direction in a rectangular Cartesian coordinate system based at the wall (Figure 1)
x_r	reattachment distance measured along the wall from the nozzle
y	transverse direction in a rectangular Cartesian coordinate system based at the wall (Figure 1)
Greek	
β	wall angle (Figure 2)

Results

Velocity distributions

To illustrate the effect of the wall angle β on the development of the velocity field, the mean nondimensional X-component velocity distributions (U/U_o) up to $X/h = 10$ are plotted in Figures 3a–c for β = 15, 30, and 45°, respectively. Unlike free jets, which have top-hat velocity distributions in the potential core, the

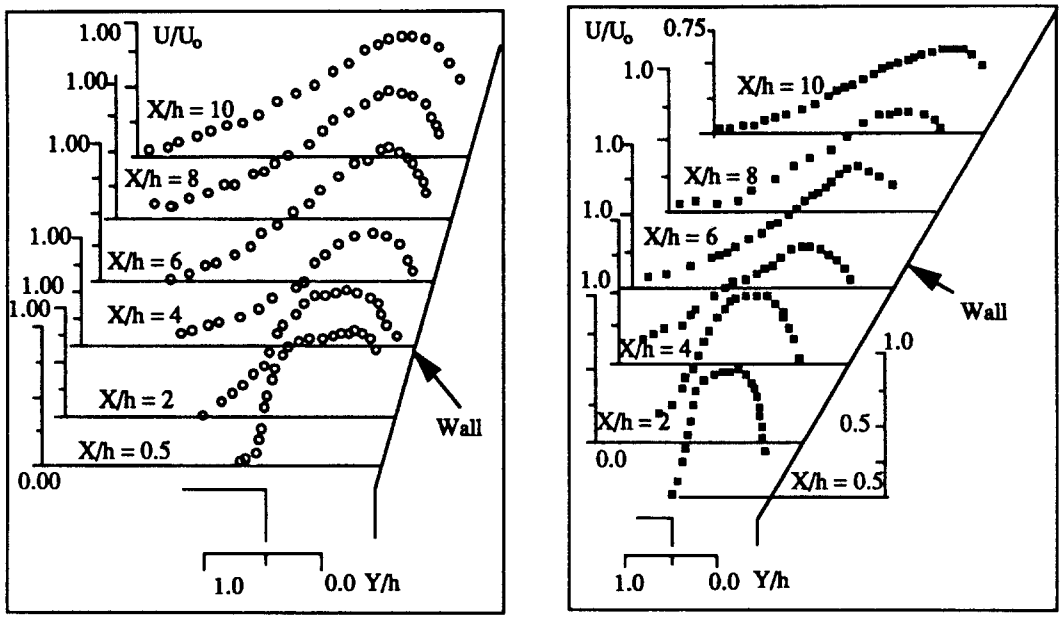

(a) β = 15° (b) β = 30°

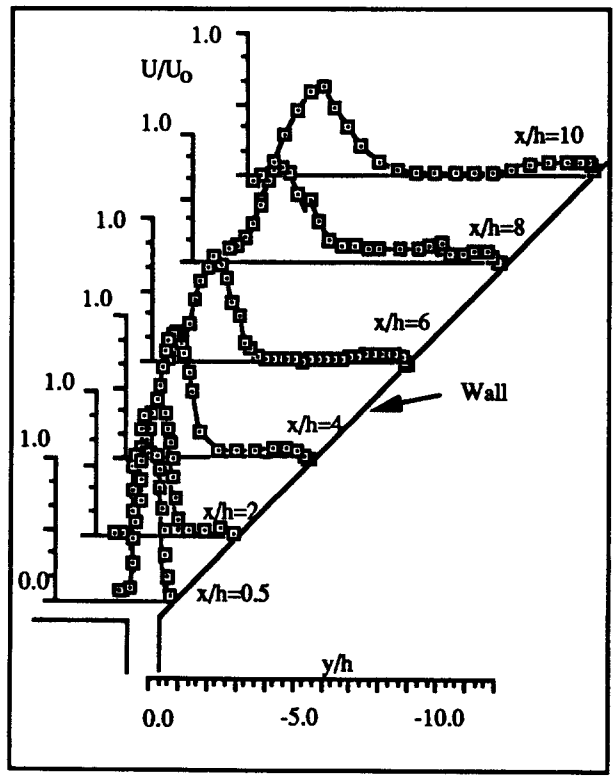

(c) β = 45°

Figure 3 Mean X-component velocity distributions: (a) β = 15°; (b) β = 30°; (c) β = 45°

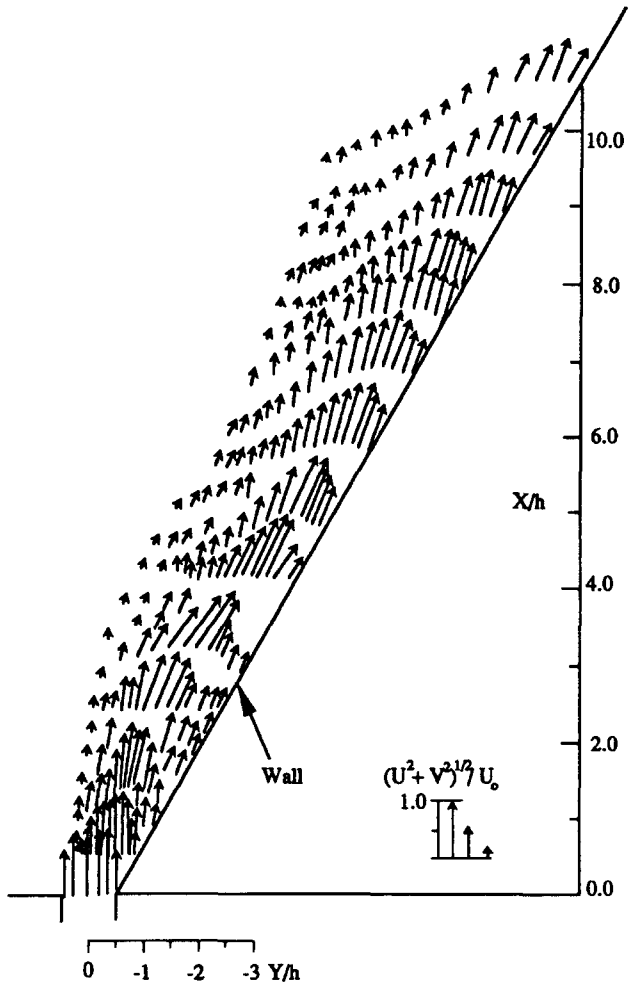

Figure 4 Velocity vector plot for $\beta = 30°$

inclined wall jet has inclined velocity distributions near the nozzle exit, indicating that the jet is deflected towards the wall. A physical explanation of the mechanism of the jet reattachment to the wall (known as the Coanda effect) has been provided by Squire (1950). Consider the jet to be fully detached from the wall immediately downstream of the nozzle. It behaves like a free jet entraining fluid from the surroundings on both sides. The fluid entrained in the confined region between the jet and the wall is accelerated near the wall, and because the flow is 2-D, a pressure

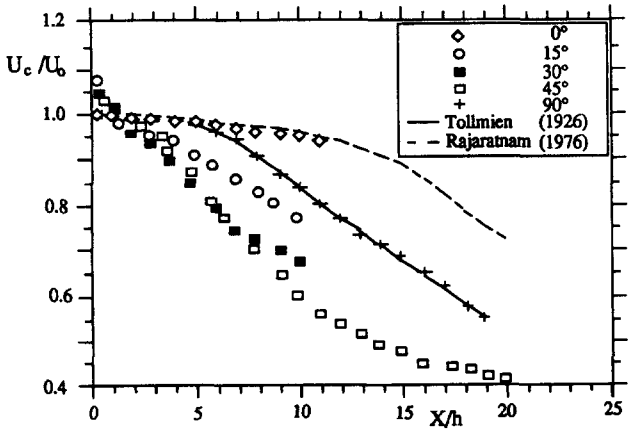

Figure 5 Centreline X-component velocity decay for various β

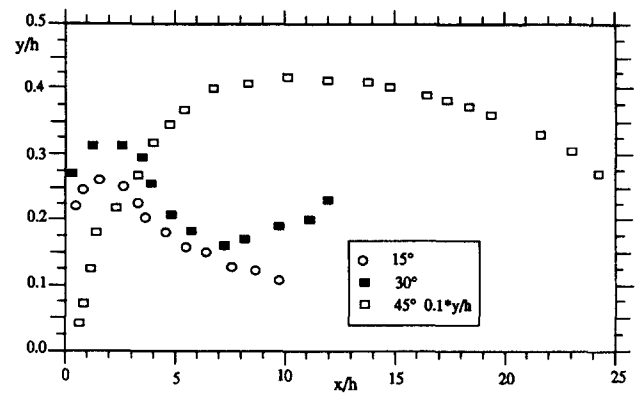

Figure 6 Locus of jet centreline for various β

lower than that of the surroundings is produced on the wall. Consequently, the jet curves towards the wall and reattaches to the wall if the wall is long enough (Figure 1).

The jet for $\beta = 15°$ appears to be slightly separated from the wall at the nozzle exit but appears to reattach by $X/h = 4$. On the other hand, the jet for $\beta = 45°$ is clearly separated from the wall at the nozzle exit, and the tendency for the jet to reattach to the wall as the flow proceeds downstream can be observed (Figure 3c). While the separation of the jet for $\beta = 30°$ at the nozzle exit is not as obvious as that for $\beta = 45°$, the deflection of the jet towards the wall is clearly illustrated (Figure 3b). Velocity vectors can be constructed from the measured X-component and Y-component velocity distributions. The initial separation of the

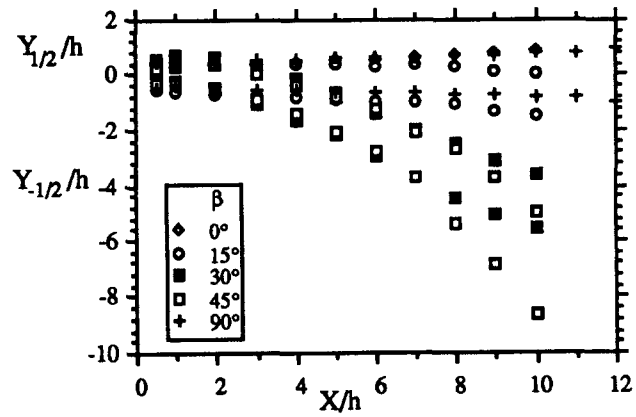

Figure 7 Jet spreading for various β

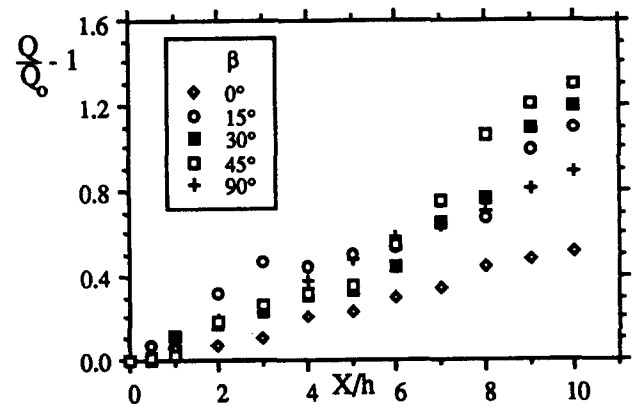

Figure 8 Jet volume entrainment for various β

jet from the wall at the nozzle exit and the curving of the jet towards the wall as the flow proceeds downstream are clearly discerned in the velocity vector plot for $\beta = 30°$ in Figure 4. It must be cautioned that hot-wire results in the recirculating flow region and close to the wall are subject to errors due to reversed flow.

Centreline velocity decay

The centreline of the jet is defined by the locus of positions of maximum X-component velocity (U_c). The variation of the mean centreline X-component velocity (U_c) with downstream distance (X/h) for various wall angles β is shown in Figure 5. The free-jet results agree fairly well with Tollmien's solution (1926), while the wall jet data show good agreement with those of Rajaratnam (1976), thus validating the measurement technique. It should be noted from Figure 5 that U_c is greater than U_o for $\beta = 15$ and 30° immediately downstream of the nozzle ($X/h < 2$). Laser Doppler anenometer-(LDA) measurements made in a 2-D plane wall jet by Schneider and Goldstein (1994) also show that U_c is 10% higher than U_o. This is because U_c is the maximum velocity at a given X, whereas, U_o is the averaged nozzle exit velocity. Owing to the presence of the wall and the deflection of the jet towards the wall, it can be seen from Figures 3a and b that the mean X-component velocity profiles in the neighbourhood

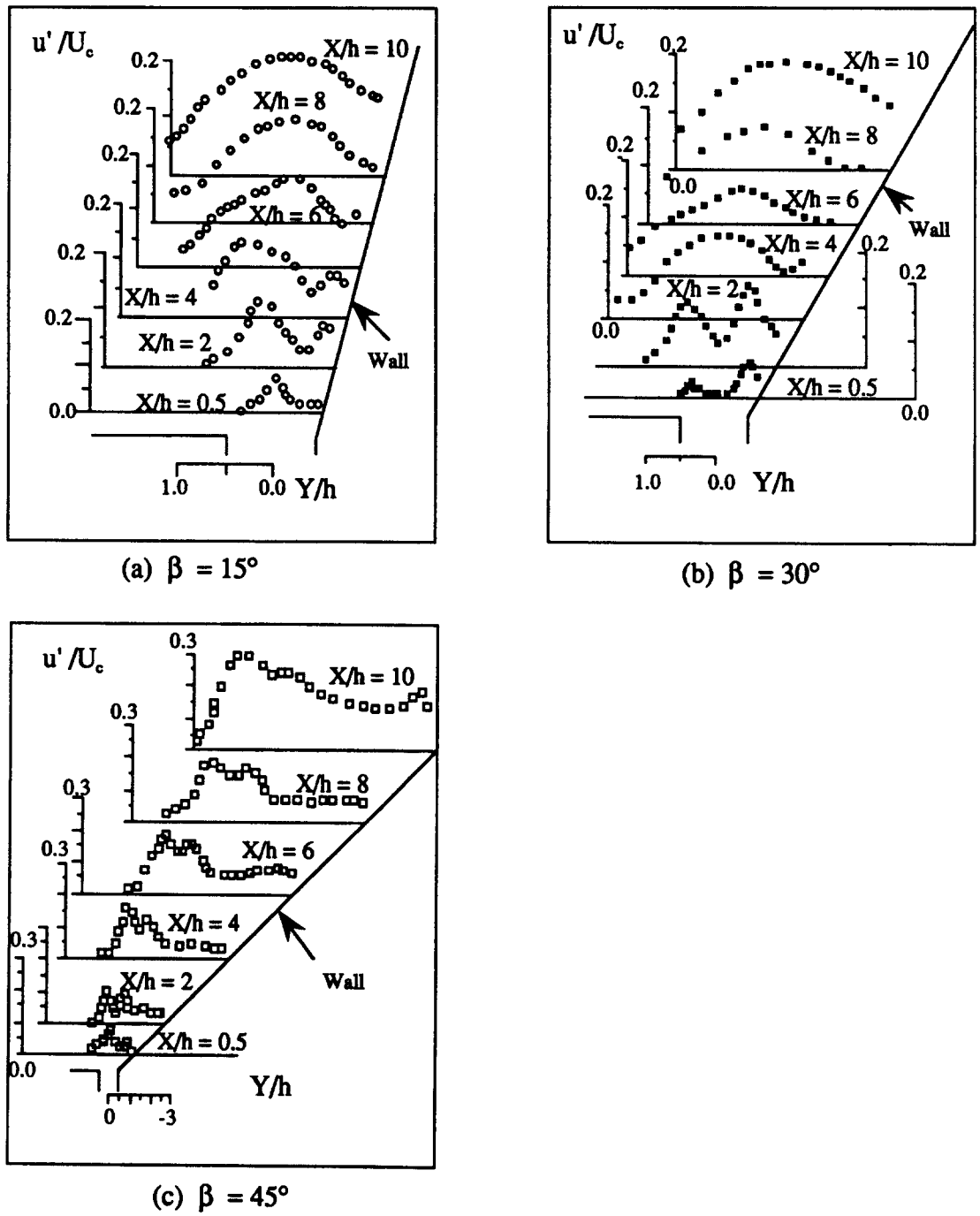

Figure 9 X-component turbulence intensity distributions; (a) $\beta = 15°$; (b) $\beta = 30°$; (c) $\beta = 45°$

immediately downstream of the nozzle are not uniform. Furthermore, due to the presence of a subatmospheric recirculation flow region close to the nozzle exit, the fluid is accelerated immediately downstream of the nozzle. Consequently, for $X/h < 2$, U_c is greater than U_o. For $\beta = 0°$, U_c occurs at a point closer to the wall than that the X-wire probe could be positioned to because of the finite size of the probe. Thus, in Figure 5, U_c for $\beta = 0°$ is actually the mean X-component velocity measured by the X-wire at the closest point to the wall within the physical constraints of the wall and the probe. For $\beta = 45°$, there is a minimal effect of the wall on U_c immediately downstream of the nozzle exit where the jet behaves almost like a free jet, as illustrated in Figure 3c, thus yielding $U_c/U_o \approx 1$.

Because a free jet entrains fluid from both sides, it spreads faster, and, therefore, it centreline velocity decays faster than that for the wall jet in the flow development region near the nozzle exit. It is interesting to note that the centreline velocity decay rate in the far field (for $X/h > 10$) is virtually the same for $\beta = 0°$ (wall jet) and 90° (free jet). As β increases from 0 to 45°, the centreline velocity decays faster, and transition from laminar to turbulent condition occurs earlier than a free jet. To illustrate the deflection of the jet centreline towards the wall, the locus of points at which the local mean X-component velocity is maximum is plotted in the (x, y) coordinates (see Figure 1) in Figure 6. As observed by Newman (1961) and as discussed above, the reattachment point increases with β. For small wall angles, such

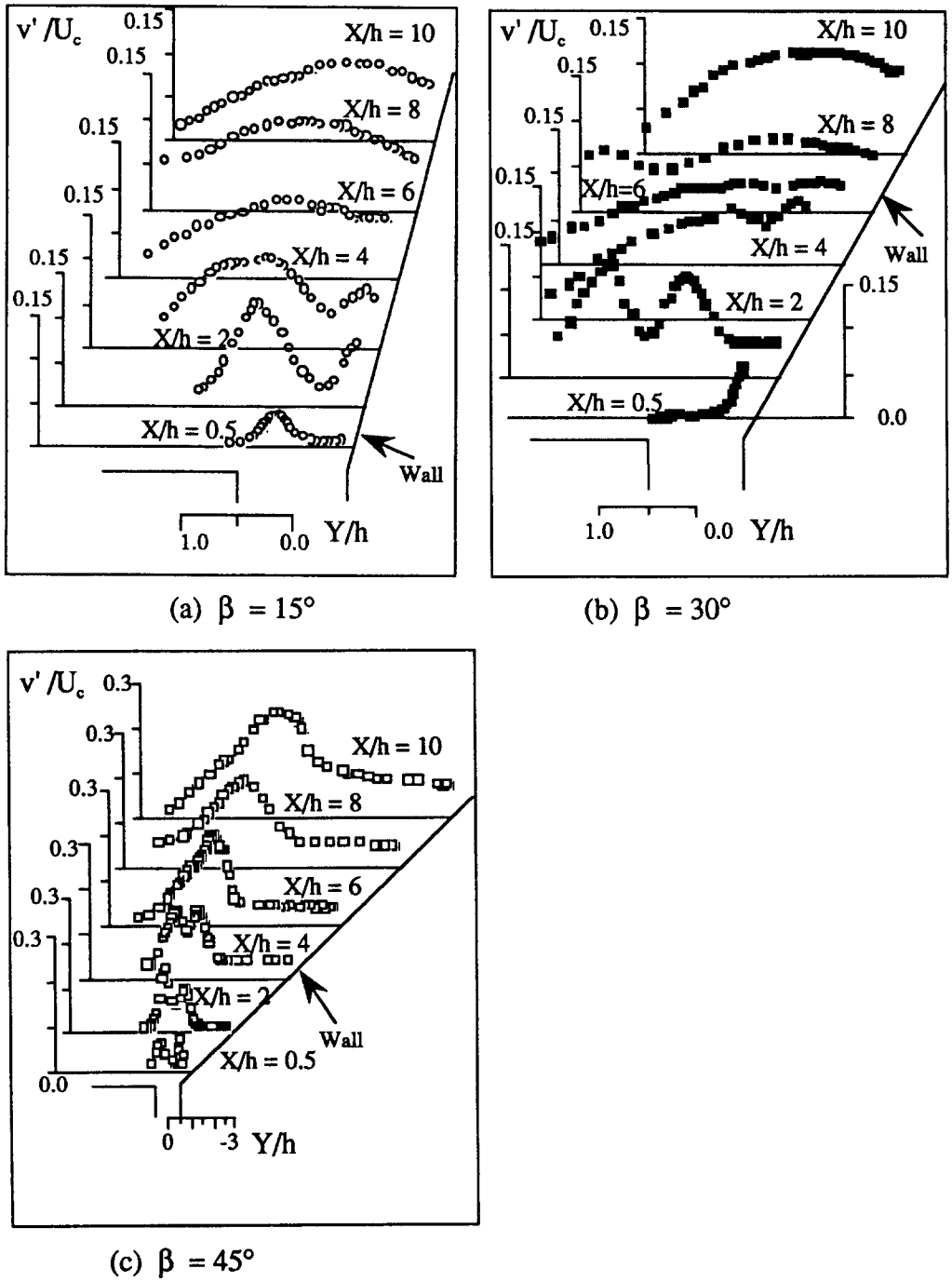

Figure 10 Y-component turbulence intensity distributions: (a) $\beta = 15°$; (b) $\beta = 30°$; (c) $\beta = 45°$

as $\beta = 15°$, it is difficult to detect the separation bubble. It is interesting to note that for $\beta = 45°$, the locus of U_c tends to form an arc, in agreement with Newman's assumption.

Jet spreading and entrainment

Figure 7 shows the variation of $Y_{1/2}/h$ and $Y_{-1/2}/h$ with X/h for various β. Results for $\beta = 0°$ (wall jet) and 90° (free jet) indicate that the jet spreading increases almost linearly in agreement with the results of Tollmein (1926). For small β such as 15°, the jet spreads mostly in the outer shear layer, and the inner shear layer development is constrained by the presence of the wall. For larger β, such as 45°, the recirculation flow region is large, and by $X/h = 10$, the jet is much wider than a free jet for the same nozzle upstream condition. These results indicate that jet spreading increases with the size of the recirculation flow region, which is dependent on β, as shown in Figures 3a–c. By integrating mean X-component velocity profiles between points where the local mean velocity $U = 0.05\ U_c$, the volume flow rate Q at a given X/h can be obtained. This is the procedure adopted for $\beta = 90°$. For $\beta = 15$ and 30°, it can be seen from Figures 3a and b that the measurement point closest to the wall is well outside the recirculating flow region, and U measured there is at least $0.25\ U_c$. Consequently, the volume flow rate for $\beta = 15$ and 30° will be underestimated. For $\beta = 45°$, it can be seen from Figure 4c that as the wall is approached, U decreases from U_c at the centreline to less than $0.05\ U_c$ outside the recirculating flow region, but U then increases in the recirculation flow region to at least about $0.1\ U_c$ and decreases towards 0 at the wall. Thus, the estimate of the volume flow rate for $\beta = 45°$ has not been affected by the reversed flow in the recirculation flow region.

The variation of volume flow entrainment, defined here as $(Q - Q_o)/Q_o$, with X/h is shown in Figure 8. Here Q_o is the volume flow rate at the nozzle exit. It can be seen that near the nozzle exit ($X/h < 4$), the entrainment for a free jet is larger than that for $\beta < 90°$, because the ambient fluid is entrained from both sides of the jet. However, as the pressure inside the recirculation flow region is reduced to below that of the surroundings with increasing X/h, the entrainment of the jet for large β such as 45° increases rapidly to above that of the free jet. The increase in volume flow entrainment by an inclined wall jet over that of a free jet was also observed by Newman (1961).

Turbulence characteristics

The spatial development of the X-component turbulence intensity (u'/U_c) with X/h is shown in Figures 9a–c for $\beta = 15$, 30, and 45°, respectively. For small β, such as 15° where the size of the recirculation flow region is small, the jet approaches that of a half jet so that there appears to be only one peak in the u'/U_c distribution. On the other hand, for large β, such as 45°, the jet is separated from the wall at the nozzle exit, and, before reattachment, two peaks located in the inner and outer shear layers are clearly discerned. As the flow reattaches to the wall and proceeds downstream, the inner shear layer merges into the wall boundary layer, with the result that the peak in the inner shear layer is no longer detectable. The spatial development of the Y-component turbulence intensity (v'/U_c) with X/h behaves in a way similar to that of the X-component turbulence intensity, as shown in Figures 10a–c for $\beta = 15$, 30, and 45°, respectively. The spatial development of Reynolds shear stress $\overline{u'v'}/U_c^2$ with X/h for various β is shown in Figures 11a–b for $\beta = 15$ and 45°, respectively. It can be seen that as β increases, $\overline{u'v'}/U_c^2$ increases. For small β, such as 15°, high values of Reynolds shear stress occur near the wall surface (Figure 11a) similar to wall jet flows. Furthermore, the Reynolds shear stress for $\beta = 15°$ is maximum at about $X/h = 4$ where flow reattachment occurs, thus indicating large momentum transfer near the reattachment point.

Comparison between hot-wire and laser Doppler anemometer measurements

Although the primary focus of this study is in the flow region outside the recirculating flow region, it is pertinent to examine

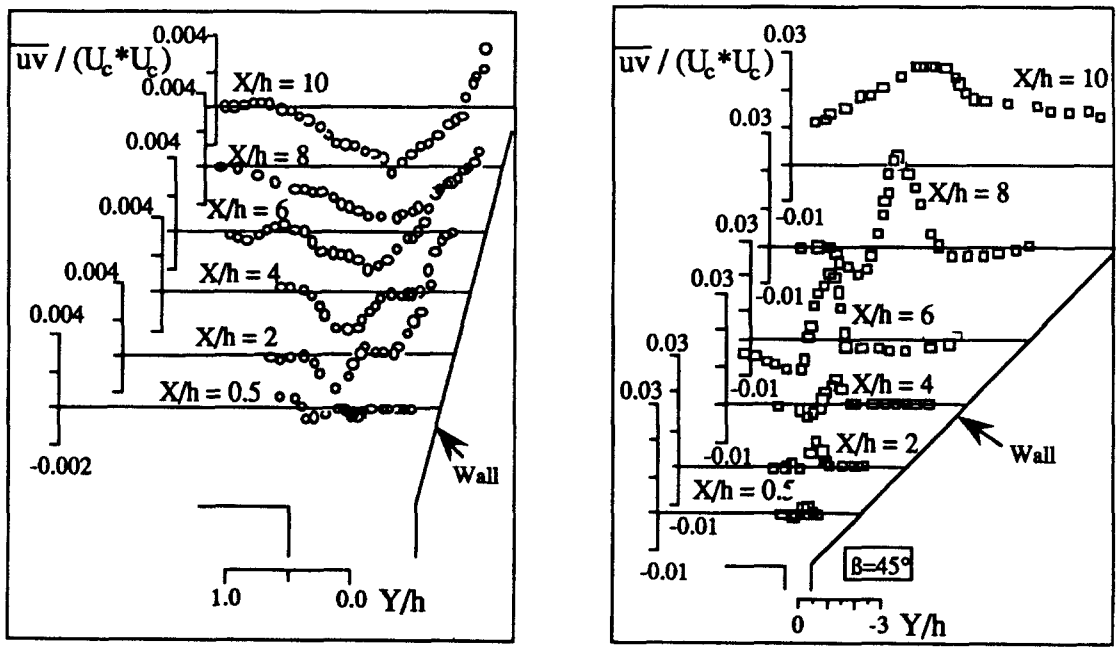

Figure 11 Reynolds shear stress distributions: (a) $\beta = 15°$; (b) $\beta = 45°$

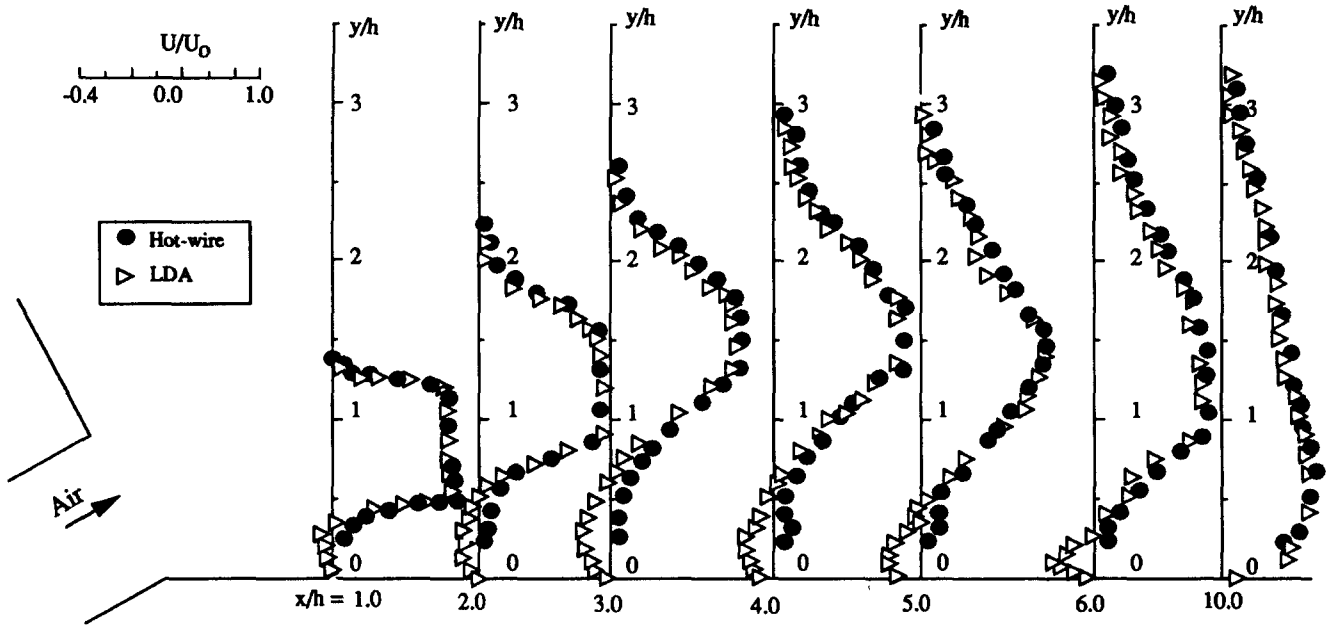

Figure 12 Comparisons of mean streamwise velocity between hot-wire and LDA measurements

the validity of hot-wire measurements. In fact, LDA measurements made by Lai and Lu (1995) for a 30° jet show that there is good agreement between results obtained by hot-wire and LDA in mean velocities, turbulence intensities, and Reynolds stress everywhere in the flow except in the recirculating flow region where conventional hot-wire techniques cannot discriminate against reversed flow. Figure 12 shows one such comparison for the spatial development of the mean streamwise velocity for an 30° jet in (x, y) coordinate system based on the wall. Results in Figure 12 certainly indicate that the hot-wire results presented in the previous sections are valid for the whole flow field except in the recirculating flow region.

Wall surface pressure distributions

Wall surface pressure distributions were made to provide some indication of the existence of a separation bubble for an inclined wall jet. Figure 13 displays the nondimensional pressure distributions $(P_\infty - P_s)/(P_0 - P_\infty)$ at a nozzle exit Reynolds number of 10,000 for $\beta = 15$, 30, and 45°, respectively. Here P_0, P_∞, and P_s refer, respectively, to the supply jet pressure, the static pressure in the surroundings, and the wall surface pressure. It can be seen that for $\beta > 10°$, there exists a separation region immediately downstream of the nozzle where the surface pressure is below that of the surroundings, thus promoting entrainment of the surrounding fluid. As the jet curves towards the wall for reattachment, the surface pressure increases to above that of the surroundings, because the fluid streamlines are not parallel to the wall, and the measured surface pressure is not truly static. Downstream of the jet reattachment point, the streamlines become parallel to the wall, and hence, the surface pressure measured is recovering to approach that of the surrounding fluid. It can be noted from Figure 13 that, consistent with the velocity measurements discussed in the velocity distributions section, the size of the separation bubble depends on β.

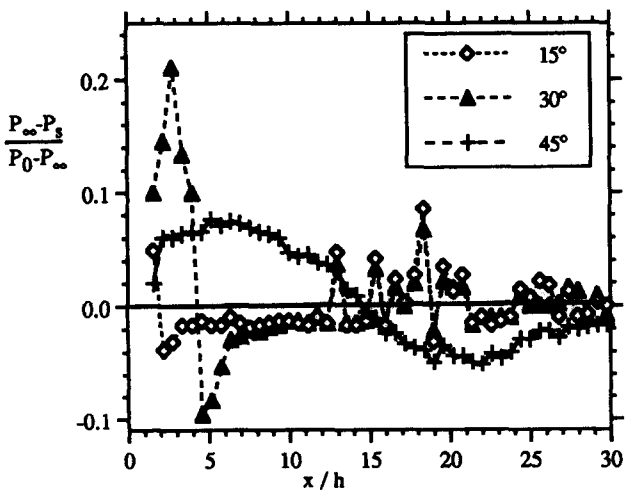

Figure 13 Wall surface pressure distribution

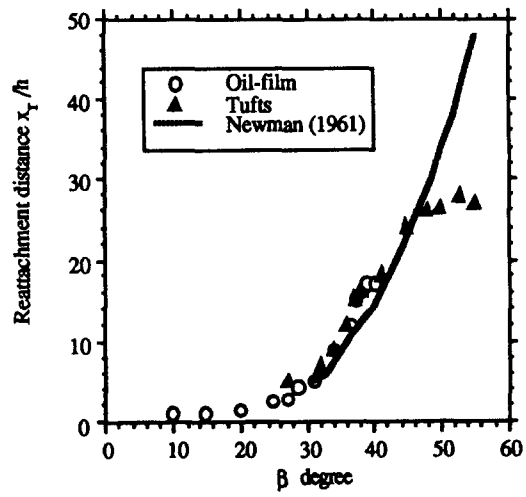

Figure 14 Variation of reattachment distance with β

Flow visualisation

Oil film and tufts techniques were used to provide an estimate of the reattachment distance of an inclined wall jet for a range of wall angles β, and smoke was used to illustrate the entrainment process. Figure 14 shows the variation of reattachment distance with β, and the results agree fairly well with those of Newman (1961). It must be pointed out that, for the oil film technique, the direction of surface oil flow depends on the shear stress at the wall. However, for large β, the wall shear stress is small, and the oil flow pattern is not clear. Thus, the oil film technique is not suitable for $\beta > 45°$. For small β, the reattachment distance can be obtained by carefully observing the movement of tiny oil particles. It has been found that in the present jet facility, the jet will not reattach to the wall if β is greater than 55°. The surface pressure distributions in Figure 13 agree, at least qualitatively, with the estimate of reattachment distance in Figure 14.

Conclusions

The velocity field for a 2-D wall jet with laminar exit condition and a nozzle exit Reynolds number of 10,000 has been studied using X-wires for various angles of inclination of the wall to the nozzle; namely, $\beta = 0$, 15, 30, 45, and 90°. Results indicate that in the range $0° \leq \beta \leq 45°$, as the wall angle β increases, both the centreline velocity decays faster, and the jet spreads faster, thus, resulting in a shorter potential core and increase in jet volume entrainment. The spatial development of mean velocity distributions is greatly affected by the size of the recirculation flow region, which is governed by the wall angle β. The variation of reattachment distance with wall angle β, in the range $10° \leq \beta \leq 55°$, has been estimated using surface pressure measurements and flow visualisation techniques and is in good agreement with the results of Newman (1961).

Acknowledgment

The second author (D. Lu) acknowledges receipt of a University College Rector's Research Scholarship.

References

Bourque, C. 1967. Reattachment of a two-dimensional jet to an adjacent flat plate. In *Adv. in Fluidics*, F. T. Brown (ed.), ASME, New York, 192–204

Bourque, C. and Newman, B. G. 1960. Reattachment of a two-dimensional incompressible jet to an adjacent flat plate. *Aeronaut. Quarterly*, **11**, 201–232

Forthmann, E. 1934. Uber turbulente Stranhlausbreitung. *Ing.-Arch.*, **5**, 42, also NACA TM789, 1936

Hsiao, F. B. and Sheu, S. S. 1994. Double row vortical structures in the near field region of a plane wall jet. *Exp. Fluids*, **17**, 291–301

Katz, Y., Horev, E. and Wygnanski, I. 1992. The forced turbulent wall jet. *J. Fluid Mech.*, **242**, 577–609

Lai, J. C. S. and Simmons, J. M. 1985. Instantaneous velocity measurements in a vane-excited plane jet. *AIAA J.*, **23**, 1157–1164

Lai, J. C. S. and Lu, D. 1995. LDA measurements of an inclined two-dimensional wall jet. *Proc. 6th Asian Congress of Fluid Mechanics*, Singapore, **2**, 1018–1021

Launder, B. E. 1983. The turbulent wall jet — Measurements and modelling. *Ann. Rev. Fluid Mech.*, **15**, 429–459

Launder, B. E. and Rodi, W. 1981. The turbulent wall jet. *Prog. Aerospace Sci.*, **19**, 81–128

Marsters, G. F. 1978. The attachment of a ventilated plane jet to an inclined plane wall. *Aeronaut. Quarterly*, 60–74

Matsuda, H., Iida, S. and Hayakawa, M. 1990. Coherent structures in a three-dimensional wall jet. *Trans ASME. J. Fluids Eng.*, **112**, 462–467

Newman, B. G. 1961. The deflection of plane jet by adjacent boundaries — Coanda effect. In *Boundary Layer and Flow Control*, G. V. Lachmann (ed.), Pergamon Press New York, 232–265

Perry, C. C. 1967. Two-dimensional jet attachment. In *Advances in Fluidics*, F. T. Brown (ed.), ASME, New York, 205–217

Rajaratnam, N. 1976. *Turbulent Jets*. Elsevier Science, New York

Schneider, M. E. and Goldstein, R. J. 1994. Laser Doppler measurement of turbulence parameters in a two-dimensional plane wall jet. *Phys. Fluids*, **6**, 3116–3129

Squire, H. B. 1950. Jet flow and its effect on aircraft. *Aircraft Eng.*, **22**, 62

Tollmien, W. 1926. Berechnung turbulenter Ausbreitungsvorgange *ZAMM*, **6**, 468–478

Zhou, M. D. and Wygnanski, I. (1993) Parameters governing the turbulent wall jet in an external stream. *AIAA* J., **31**, 848–853